Instabilities in passive and active optical systems with a Gaussian transverse intensity profile

L. A. Lugiato, R. J. Horowicz,* and G. Strini
Dipartimento di Fisica dell'Università degli Studi di Milano, via Celoria 16, I-20133 Milano, Italy

L. M. Narducci
Physics Department, Drexel University, Philadelphia, Pennsylvania 19104
(Received 9 March 1984)

In this paper we analyze the steady-state and stability properties of bistable optical systems, lasers with an injected signal, and ordinary free-running lasers. The starting point of our study is a unified model of a ring cavity containing a finite-size cylindrical sample of homogeneously broadened two-level atoms, and capable of supporting a single field mode with a Gaussian transverse profile. After solving the equations of motion in the steady state, we carry out a linear stability analysis of the stationary solutions, identify the domains of unstable operation of each of the three systems, and compare in detail the results of this work with those of earlier plane-wave uniform-field calculations. In the case of the laser with an injected signal, we find a significant enhancement of the instability domain relative to the plane-wave limit. A similar conclusion holds for mixed absorptive and dispersive optical bistability, although the enhancement of the domain of instability is less pronounced. Unstable behavior is predicted to occur for experimentally accessible values of the bistability parameter, and to be favored by the absence of bistability and by the selection of atomic and cavity detunings having opposite signs. This configuration ensures that the instability will be responsible for the emergence of undamped output pulsations of the type that will make the bistable system behave as an optical clock.

I. INTRODUCTION

The unstable behavior of certain optical systems has attracted considerable attention not only because of the widespread current interest in the general area of nonlinear dynamics, but also because optical instabilities are viewed as a practical working principle for such devices as optical clocks and other all-optical logic components. With very few exceptions[1-5] most instability problems in quantum optics have been analyzed in the context of the plane-wave and infinite active medium approximation. Recently we have begun to see evidence that a nonuniform field transverse profile can alter the predictions of the plane-wave theory not only quantitatively, but qualitatively as well. This fact has been made especially obvious by the results of Refs. 2 and 4. Thus, for example, the Ikeda instability[6] which, in the plane-wave approximation, is the source of a period doubling sequence and chaotic oscillations, develops a different route to chaos if the input field has a Gaussian transverse profile.[2] Other instabilities of the plane-wave theory in the presence of a Gaussian field profile are even suppressed altogether.[4]

In dealing with transverse effects, one must distinguish between the cases in which the cavity has plane or spherical mirrors. In this paper we consider a ring cavity with spherical mirrors containing a collection of two-level atoms. If an input field is present, we assume that this is matched to the fundamental TEM_{00} mode of the resonator. Our analysis is based on the simplest possible model and it involves the following approximations.

(i) We consider the mean field limit $\alpha L \ll 1$, $T \ll 1$ with $\alpha L/T$ constant and arbitrary;[7] as usual, α represents the absorption coefficient per unit length of the atomic sample, L the length of the medium, and T the transmission coefficient of the mirrors. We assume, in addition, that the evolution of the system takes place over a time scale which is much longer than a single cavity round-trip time.

(ii) We assume that the transverse profile of the electric field in the *filled* cavity corresponds to the TEM_{00} mode. This appears to be a reasonable approximation in the mean field limit.

(iii) We assume that the Fresnel number $w_0^2/\lambda L$ is large so that the beam radius is practically constant over the length of the atomic sample; w_0 is the beam waist and λ is the wavelength of the radiation.

As a consequence of points (i) and (ii), this is a one-mode model whose equations of motion were derived from first principles in Ref. 4. Studies of its steady-state properties have appeared in Refs. 8 and 9.

Assumption (ii) requires some comments. Because it imposes a time-independent TEM_{00} profile for the electric field, it cannot be expected to hold over the entire range of parameters of practical interest. In fact, the occurrence of a laser instability in which transverse modes, other than TEM_{00}, play an essential role is documented in Ref. 5. We note, in addition, that this instability does not even have a counterpart in the plane-wave limit because it arises in the rate-equation approximation. Our present strategy is to concentrate on instabilities which are known to occur in the plane-wave limit and to evaluate the role played in the context of our model by a more realistic field profile. We expect that our one-transverse mode assumption should be satisfactory in at least two situations:

(a) when all the other modes are sufficiently detuned from the carrier frequency of the incident field (or, in the case of the free-running laser, from the center of the gain profile) or (b) when the losses of all the other modes are large enough to keep their amplitudes at a negligible level. In the absence of arguments for neglecting higher-order transverse modes, a compelling justification for the stability analysis performed in this work is that our model allows an analytic handling of the steady-state and stability properties over the entire parameter space. The exact equations of motion without the one-mode assumption can, apparently, be studied only by numerical methods, a task which is time consuming and of uncertain effectiveness. Thus, as a second step, and building from the knowledge gained from the present model, do we plan to study a more general setting.

At present, we consider simultaneously three of the most interesting systems in quantum optics: mixed absorptive and dispersive optical bistability (OB), the laser with an injected signal (LIS), and the free running laser (FRL) with nonzero detuning between the centers of the atomic and cavity frequencies. In all cases the atoms are assumed to be homogeneously broadened. As our first step, we consider the stability of the stationary solutions. In subsequent contributions, we plan to analyze the equations of motion of our model and to investigate the nature of the pulsations that emerge under unstable conditions.

In Sec. II we describe the model which forms the starting point of our analysis. We construct its stationary solutions in Sec. III and derive, in Sec. IV, the basic stability conditions; in Sec. IV we also discuss the connection between our results and the sidemode gain approach. Sections V—VII illustrate the type of instabilities that arise in the presence of a Gaussian transverse profile for OB, LIS, and FRL, respectively. Our results are summarized and discussed in Sec. VIII.

II. GAUSSIAN ONE-MODE MODEL FOR ACTIVE AND PASSIVE SYSTEMS

A unidirectional ring cavity of the type shown schematically in Fig. 1 contains a cylindrical atomic sample of length L and radius R. Because of the cylindrical symmetry, the only relevant transverse variable is the radial coordinate r whose range of variation is $0 \le r \le R$. The one-mode model is characterized by the following equations of motion:[4]

$$\kappa^{-1}\frac{d}{dt}\tilde{f}_0(t) = -\left[\tilde{f}_0(1+i\theta)-y+2C\int_0^{R/w_0} d\vec{r}\,4\vec{r}\exp(-\vec{r}^2)P(\vec{r},t)\right], \tag{1a}$$

$$\gamma_\perp^{-1}\frac{\partial}{\partial t}P(\vec{r},t) = D(\vec{r},t)\tilde{f}_0(t)\exp(-\vec{r}^2)-(1+i\Delta)P(\vec{r},t), \tag{1b}$$

$$\gamma_\parallel^{-1}\frac{\partial}{\partial t}D(\vec{r},t) = -\tfrac{1}{2}[P(\vec{r},t)\tilde{f}_0^*(t)+P^*(\vec{r},t)\tilde{f}_0(t)]\exp(-\vec{r}^2)-D(\vec{r},t)+1. \tag{1c}$$

The normalized radial variable is defined as $\vec{r}=r/w_0$, w_0 is the beam waist, and $\tilde{f}_0(t)$ and y are defined as

$$\tilde{f}_0(t)=\sqrt{2/\pi}\frac{1}{w_0}f_0(t),\quad y=\sqrt{2/\pi}\frac{1}{w_0}y_0. \tag{2}$$

The parameters y_0 and f_0 denote the normalized amplitudes of the incident field and of the fundamental TEM_{00} cavity mode, respectively. $P(\vec{r},t)$ and $D(\vec{r},t)$ are scaled quantities corresponding to the macroscopic atomic polarization and population difference at a distance r from the axis of the system. The equations of motion for $\tilde{f}_0^*(t)$ and $P^*(\vec{r},t)$ are the complex conjugate equations (1a) and (1b); κ is the field damping rate $cT/\mathcal{L}$, where $\mathcal{L}$ is the length of the ring cavity and T is the mirrors' transmission coefficient; $\gamma_\parallel=T_1^{-1}$ and $\gamma_\perp=T_2'^{-1}$ are the longitudinal and transverse atomic relaxation rates, respectively. The parameter C is defined by

$$C=-\frac{\alpha L\sigma}{2T}, \tag{3}$$

where α is the unsaturated absorption coefficient, and σ ($|\sigma|<1$) is the unsaturated population inversion per atom created by the pump. In the laser case, σ is positive and $|C|$ represents the gain parameter. In the presence of an injected signal one has $y\neq 0$, while for the free-running laser y must be set equal to zero. In the case of OB one has $\sigma=-1$ (no pump) and C coincides with the usual bistability parameter.

For OB and LIS, θ and Δ denote the cavity and atomic detuning parameters, respectively,

$$\theta=\frac{\omega_C-\omega_0}{\kappa},\quad \Delta=\frac{\omega_A-\omega_0}{\gamma_\perp}. \tag{4}$$

ω_0 is the frequency of the incident field and ω_C the frequency of the cavity mode, while ω_A is the atomic transi-

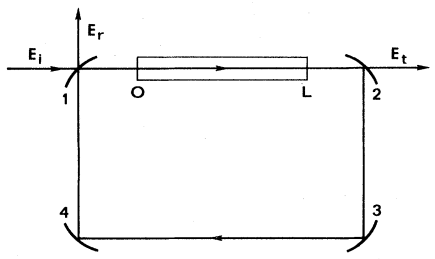

FIG. 1. Schematic representation of a unidirectional ring cavity with spherical mirrors. E_i, E_t, and E_r are the incident, transmitted, and reflected fields, respectively. Mirrors 3 and 4 have 100% reflectivity. Mirrors 1 and 2 have transmittivity T.

tion frequency. In the case of the FRL, we identify ω_0 as the laser oscillation frequency in the nontrivial stationary state. As shown in Sec. III, the laser's oscillation frequency is still given by the well-known mode-pulling formula, even in the presence of a transverse Gaussian field profile. Thus θ and Δ are no longer independent of each other but are linked by the relation $\Delta=-\theta$.[10]

For the sake of comparison, we recall the equations of motion for the mean field model in the plane-wave limit:[11]

$$\kappa^{-1}\frac{d}{dt}f=-[(1+i\theta)f-y+2CP]\ , \tag{5a}$$

$$\gamma_\perp^{-1}\frac{d}{dt}P=Df-(1+i\Delta)P\ , \tag{5b}$$

$$\gamma_\parallel^{-1}\frac{d}{dt}D=-\tfrac{1}{2}(Pf^*+P^*f)-D+1\ , \tag{5c}$$

where y and f are the normalized amplitudes of the incident and cavity fields, respectively. In Eqs. (5) the field and atomic variables are only functions of time.

III. STEADY-STATE SOLUTIONS

In steady state the atomic variables are given by

$$P^{\rm st}(\vec{r})=\frac{(1-i\Delta)\tilde{f}_0^{\rm st}\exp(-\vec{r}^{\,2})}{1+\Delta^2+|\tilde{f}_0^{\rm st}|^2\exp(-2\vec{r}^{\,2})}\ , \tag{6a}$$

$$D^{\rm st}(\vec{r})=\frac{1+\Delta^2}{1+\Delta^2+|\tilde{f}_0^{\rm st}|^2\exp(-2\vec{r}^{\,2})}\ , \tag{6b}$$

and, after setting $x=|\tilde{f}_0^{\rm st}|$, the field equation can be cast into the form

$$y^2=x^2\left[\left[1+\frac{2C}{x^2}g(x^2)\right]^2+\left[\theta-\frac{2C\Delta}{x^2}g(x^2)\right]^2\right]\ , \tag{7}$$

where[1,4,8,9]

$$g(x^2)=\ln\left[\frac{1+\Delta^2+x^2}{1+\Delta^2+x^2\exp[-2(R/w_0)^2]}\right]\ . \tag{8}$$

In the case of the FRL ($y=0$), Eq. (7) implies the identity

$$\Delta=-\theta \tag{9}$$

as anticipated in the preceding section. By taking the definitions of Δ and θ into account, one finds, from Eq. (9), the well-known mode-pulling formula

$$\omega_0=\frac{\kappa\omega_A+\gamma_\perp\omega_C}{\kappa+\gamma_\perp}\ . \tag{10}$$

The steady-state output field is given by the solution of the transcendental equation

$$1=-\frac{2C}{x^2}g(x^2)\ . \tag{11}$$

In addition, the state equation (7) is satisfied by the trivial solution $x=0$. From Eq. (11) we see that the laser threshold is characterized by the following value of the gain parameter:

$$|C|=(1+\theta^2)/2\xi\ , \tag{12}$$

where

$$\xi=1-\exp[-2(R/w_0)^2]\ . \tag{13}$$

The phase of the steady-state field $\tilde{f}_0^{\rm st}$ of course remains arbitrary.

In the plane-wave limit, starting from Eqs. (5) we obtain the following steady-state values of the atomic variables:

$$P^{\rm st}=\frac{(1+i\Delta)f^{\rm st}}{1+\Delta^2+|f^{\rm st}|^2}\ , \tag{14a}$$

$$D^{\rm st}=\frac{1+\Delta^2}{1+\Delta^2+|f^{\rm st}|^2}\ . \tag{14b}$$

After setting $x=|f^{\rm st}|$, Eqs. (7)–(11) retain their structure even in the plane-wave limit. The function $g(x^2)$, however, is given by[11]

$$g(x^2)=x^2/(1+\Delta^2+x^2)\ . \tag{15}$$

The laser threshold occurs at a value of the gain parameter given by

$$|C|=(1+\theta^2)/2\ . \tag{16}$$

Thus on comparing Eqs. (12) and (16) we see that the threshold gain in the case of the Gaussian profile coincides with that of the plane-wave theory, apart from the simple rescaling factor ξ [Eq. (13)].

We consider now the limit $R/w_0\to 0$ of the Gaussian theory. In this situation the atomic sample interacts only with the central part of the Gaussian beam, so that one may expect to recover the results of the plane-wave theory. One has to be careful, however, because the limit $R/w_0\to 0$ by itself leads to the empty cavity configuration. On the other hand, in the double limit

$$R/w_0\to 0,\quad C\to\infty \tag{17}$$

with

$$C'=2C(R/w_0)^2 \tag{18}$$

constant and arbitrary, one does indeed recover the plane-wave results, as one can readily verify from Eqs. (8) and (15), if one replaces C with C'. It must be noted that a direct comparison of the steady-state values of x in the Gaussian and plane-wave theories is not entirely meaningful because x corresponds to the peak value of the field profile. A more meaningful comparison, instead, is the following. In the Gaussian case, the power W emitted by a sample of radius R can be estimated as follows, using Eq. (2) and the definition of x:

$$\begin{aligned}W_G&\propto 2\pi\int_0^R r\,dr\,x_G^2 e^{-2(r/w_0)^2}\\&=(\pi/2)w_0^2\{1-\exp[-2(R/w_0)^2]\}x_G^2\\&=(\pi/2)w_0^2\xi x_G^2\ .\end{aligned}$$

In the plane-wave case, instead, one has

$$W_{\rm pw}\propto\pi R^2 x_{\rm pw}^2\ .$$

In the double limit of Eq. (17) in which, as shown, the

value of x_G converges to that of x_{pw}, the ratio W_G/W_{pw} approaches unity. In the opposite limit, $R/w_0 \to \infty$, the ratio W_G/W_{pw} vanishes because the plane-wave energy density is uniform everywhere in space.

Even if a direct comparison of the values of x in the Gaussian and plane-wave cases is not correct, it is still meaningful to compare quantities such as the laser or the bistability thresholds, or features such as the presence or the absence of an instability for the same values of the parameters. For example, a remarkable feature of OB is that, in the limit $R/w_0 \to \infty$, the bistability threshold C_{thr} for fixed values of Δ and θ turns out to be markedly larger than in the plane-wave case.

IV. LINEAR STABILITY ANALYSIS

In order to study the stability of the stationary solutions, we introduce the deviations from the steady state,

$$\begin{aligned} \delta f(t) &= \tilde{f}_0(t) - \tilde{f}_0^{st} , \\ \delta P(\vec{r},t) &= P(\vec{r},t) - P^{st}(\vec{r}) , \\ \delta D(\vec{r},t) &= D(\vec{r},t) - D^{st}(\vec{r}) , \end{aligned} \tag{19}$$

and linearize Eqs. (1) around the steady-state values of the field and atomic variables. The resulting linear equations are

$$\kappa^{-1}\frac{d}{dt}\delta f(t) = -\left[\delta f(1+i\theta) + 2C\int_0^{R/w_0} d\vec{r}\, 4\vec{r}\exp(-r^2)\delta P(\vec{r},t)\right] , \tag{20a}$$

$$\gamma_\perp^{-1}\frac{\partial}{\partial t}\delta P(\vec{r},t) = [D^{st}(\vec{r})\delta f(t) + \tilde{f}_0^{st}\delta D(\vec{r},t)]\exp(-\vec{r}^2) - (1+i\Delta)\delta P(\vec{r},t) , \tag{20b}$$

$$\gamma_{\parallel}^{-1}\frac{\partial}{\partial t}\delta D(\vec{r},t) = -\tfrac{1}{2}[P^{st}(\vec{r})\delta f^*(t) + \tilde{f}_0^{*st}\delta P(\vec{r},t) + P^{*st}(\vec{r})\delta f(t) + \tilde{f}_0^{st}\delta P^*(\vec{r},t)]\exp(-\vec{r}^2) - \delta D(\vec{r},t) . \tag{20c}$$

Next we seek solutions of Eqs. (20) in the form

$$\begin{Bmatrix} \delta f(t) \\ \delta f^*(t) \\ \delta P(\vec{r},t) \\ \delta P^*(\vec{r},t) \\ \delta D(\vec{r},t) \end{Bmatrix} = \exp(\lambda t) \times \begin{Bmatrix} \delta f^{(0)} \\ \delta f^{*(0)} \\ \delta P^{(0)}(\vec{r}) \\ \delta P^{*(0)}(\vec{r}) \\ \delta D^{(0)}(\vec{r}) \end{Bmatrix} \tag{21}$$

following the procedure outlined in the Appendix. We are especially interested in locating the boundary of the stability domain, where $\mathrm{Re}\lambda = 0$. Thus, we set

$$\lambda = i\nu, \quad \nu \text{ real} \tag{22}$$

and, after some lengthy but elementary steps, we obtain the coupled linear homogeneous equations

$$\left[i\frac{\tilde{\nu}}{\tilde{\kappa}} + 1 + i\theta\right]\delta f^{(0)} + 2C[\mathscr{A}(\tilde{\nu},x,\Delta,\tilde{\gamma})\delta f^{(0)} + (\tilde{f}_0^{st})^2\mathscr{B}(\tilde{\nu},x,\Delta,\tilde{\gamma})\delta f^{*(0)}] = 0 , \tag{23a}$$

$$\left[i\frac{\tilde{\nu}}{\tilde{\kappa}} + 1 + i\theta\right]\delta f^{*(0)} + 2C[\mathscr{A}(\tilde{\nu},x,-\Delta,\tilde{\gamma})\delta f^{*(0)} + (\tilde{f}_0^{*st})^2\mathscr{B}(\tilde{\nu},x,-\Delta,\tilde{\gamma})\delta f^{(0)}] = 0 , \tag{23b}$$

where

$$\tilde{\nu} = \frac{\nu}{\gamma_\perp}, \quad \tilde{\kappa} = \frac{\kappa}{\gamma_\perp}, \quad \tilde{\gamma} = \frac{\gamma_{\parallel}}{\gamma_\perp} . \tag{24}$$

The functions $\mathscr{A}$ and $\mathscr{B}$ are displayed in full in the Appendix.

In the plane-wave limit, with Eqs. (5) as the starting point, the field fluctuation equations retain the same form as Eqs. (23), of course with different functions $\mathscr{A}$ and $\mathscr{B}$. Actually, in this limit, the linear stability analysis leads to a simple fifth-order algebraic equation for λ which can be studied by standard methods such as the Routh-Hurwitz criterion.[12] We choose not to pursue this simpler line of investigation for the plane-wave case so as to keep our handling of both the Gaussian and plane-wave configurations as close as possible to one another.

Quite generally, then, the condition that ensures the existence of nontrivial solutions for Eqs. (23) is

$$\left[i\frac{\tilde{\nu}}{\tilde{\kappa}} + 1 + i\theta + 2C\mathscr{A}(\tilde{\nu},x,\Delta,\tilde{\gamma})\right] \times \left[i\frac{\tilde{\nu}}{\tilde{\kappa}} + 1 - i\theta + 2C\mathscr{A}(\tilde{\nu},x,-\Delta,\tilde{\gamma})\right] = 4C^2x^4\mathscr{B}(\tilde{\nu},x,\Delta,\tilde{\gamma})\mathscr{B}(\tilde{\nu},x,-\Delta,\tilde{\gamma}) . \tag{25}$$

In terms of the two auxiliary functions

$$\mathscr{A}'(\tilde{\nu},x,\Delta,\tilde{\gamma})=\tfrac{1}{2}[\mathscr{A}(\tilde{\nu},x,\Delta,\tilde{\gamma})+\mathscr{A}(\tilde{\nu},x,-\Delta,\tilde{\gamma})]\ , \tag{26}$$
$$\mathscr{A}''(\tilde{\nu},x,\Delta,\tilde{\gamma})=\tfrac{1}{2}[\mathscr{A}(\tilde{\nu},x,\Delta,\tilde{\gamma})-\mathscr{A}(\tilde{\nu},x,-\Delta,\tilde{\gamma})]\ ,$$

Eq. (25) can also be written in the form

$$\left[i\frac{\tilde{\nu}}{\tilde{\kappa}}+1+2C\mathscr{A}'(\tilde{\nu},x,\Delta,\tilde{\gamma})\right]^2$$
$$=4C^2x^4\mathscr{B}(\tilde{\nu},x,\Delta,\tilde{\gamma})\mathscr{B}(\tilde{\nu},x,-\Delta,\tilde{\gamma})$$
$$-[\theta-i2C\mathscr{A}''(\tilde{\nu},x,\Delta,\tilde{\gamma})]^2\ . \tag{27}$$

Hence, after setting

$$\mathscr{F}(\tilde{\nu},x,\Delta,\tilde{\gamma},C,\theta)$$
$$\equiv 4C^2x^4\mathscr{B}(\tilde{\nu},x,\Delta,\tilde{\gamma})\mathscr{B}(\tilde{\nu},x,-\Delta,\tilde{\gamma})$$
$$-[\theta-i2C\mathscr{A}''(\tilde{\nu},x,\Delta,\tilde{\gamma})]^2\ , \tag{28}$$

we finally obtain

$$i\frac{\tilde{\nu}}{\tilde{\kappa}}+1+2C\mathscr{A}'(\tilde{\nu},x,\Delta,\tilde{\gamma})=\pm\mathscr{F}^{1/2}(\tilde{\nu},x,\Delta,\tilde{\gamma},c,\theta)\ . \tag{29}$$

It will be convenient to analyze this result in terms of its real and imaginary parts:

$$1=\mathscr{G}_{\pm}(\tilde{\nu},x,\Delta,\tilde{\gamma},C,\theta)\ , \tag{30a}$$
$$\tilde{\nu}=\tilde{\kappa}\mathscr{D}_{\pm}(\tilde{\nu},x,\Delta,\tilde{\gamma},C,\theta)\ , \tag{30b}$$

where the functions $\mathscr{G}_{\pm}$ and $\mathscr{D}_{\pm}$ are defined by

$$\mathscr{G}_{\pm}(\tilde{\nu},x,\Delta,\tilde{\gamma},C,\theta)=\mathrm{Re}[\pm\mathscr{F}^{1/2}(\tilde{\nu},x,\Delta,\tilde{\gamma})$$
$$-2C\mathscr{A}'(\tilde{\nu},x,\Delta,\tilde{\gamma})]\ , \tag{31a}$$
$$\mathscr{D}_{\pm}(\tilde{\nu},x,\Delta,C,\theta)=\mathrm{Im}[\pm\mathscr{F}^{1/2}(\tilde{\nu},x,\Delta,\tilde{\gamma})$$
$$-2C\mathscr{A}'(\tilde{\nu},x,\Delta,\tilde{\gamma})]\ . \tag{31b}$$

The plus or minus signs must be selected concurrently in Eqs. (30a) and (30b). Note that the functions $\mathscr{G}_{\pm}$ and $\mathscr{D}_{\pm}$ depend only on the modulus x of the stationary field $\tilde{f}_0^{\mathrm{st}}$ and not on its phase. This is in line with the fact that for the case of an ordinary laser ($y=0$) the choice of the phase of $\tilde{f}_0^{\mathrm{st}}$ is arbitrary.

We now discuss how Eqs. (30a) and (30b) are to be used if one wants to identify the stability boundary.

(i) Consider first the cases of OB and LIS, where the independent parameters are $y,\Delta,\tilde{\kappa},\tilde{\gamma},C$. In place of y, it is more convenient to use x as an independent parameter with the relation between y and x being provided by the state equation (7). In the following, we fix all parameters except for x and determine the existence and location of the stability boundary as functions of the modulus of the transmitted field. In the case of the FRL the independent parameters are $\Delta,\theta,\tilde{\kappa},\tilde{\gamma},C$. Instead of C, here also we select x as an independent parameter; the link between C and x is provided by the state equation (11). Again, we study the stability of the FRL as a function of x, holding all the other parameters fixed. Note that $\tilde{\kappa}$ does not appear at all in Eq. (30a), while it enters Eq. (30b) as a simple multiplicative factor.

(ii) For the sake of definiteness, consider Eqs. (30a) and (30b) with positive signs and with all values of the parameters fixed with the exception of x. For a selected value of x, Eq. (30b) can be solved graphically with respect to $\tilde{\nu}$ by seeking the intersect of the curve $\kappa\mathscr{D}_+(\tilde{\nu})$ with the 45° line. Let $\bar{\nu}(x)$ denote the solution obtained in this fashion. Obviously, $-\bar{\nu}(x)$ is also a solution because both $\mathscr{D}_+$ and $\mathscr{D}_-$ are odd functions of $\tilde{\nu}$, while $\mathscr{G}_+$ and $\mathscr{G}_-$ are even. If the value of $\mathscr{G}_+(\tilde{\nu},x,\Delta,\tilde{\gamma},C,\theta)$ is exactly unity for $\tilde{\nu}=\bar{\nu}(x)$, the selected value of x lies on the stability boundary. If not, suppose for the sake of definiteness that $\mathscr{G}_+(\bar{\nu}(x),x,\Delta,\tilde{\gamma},C,\theta)$ is smaller than unity [Fig. 2(a)]. In this case, one can gradually vary x until $\mathscr{G}_+>1$ [Fig. 2(c)]. As both $\mathscr{G}$ and $\mathscr{D}$ are continuous functions of x and $\bar{\nu}$, it is certain that some intermediate value of x will exist such that $\mathscr{G}_+(\bar{\nu}(x),x,\Delta,\tilde{\gamma},C,\theta)=1$ [Fig. 2(b)]. Thus, by repeated applications of this procedure, all the boundary values of x can be determined with excellent accuracy. The value of $\bar{\nu}(x)$ at the boundary coincides with the oscillation frequency of the solution that bifurcates from the stationary state at the boundary itself. The same argument applies with respect to the second pair of functions $\mathscr{G}_-$ and $\mathscr{D}_-$.

Two remarks are appropriate at this point. The first concerns the values of $\mathscr{G}$ and $\mathscr{D}$ for $\tilde{\nu}=0$. In this case, consider Eqs. (20) in the limit of adiabatic elimination of the atomic variables [this corresponds to setting the time derivatives in Eqs. (20b) and (20c) both equal to zero]. It is now easy to verify that the ansatz (21) leads to a

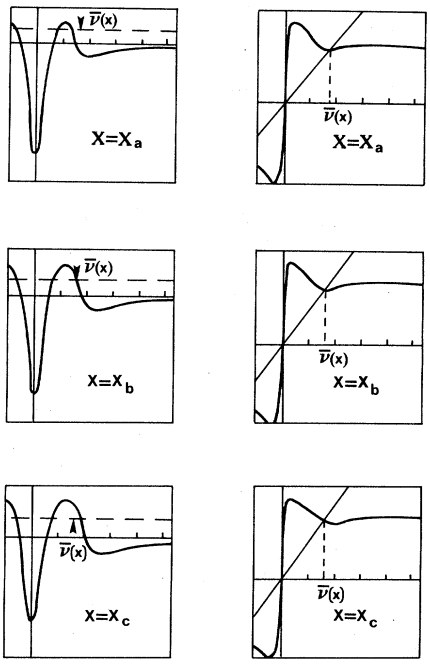

FIG. 2. Graphical identification of the stability boundary (see text). The figures on the left-hand side display the "gain" function $\mathscr{G}(\tilde{\nu})$ for three different values of x ($x_a<x_b<x_c$), with all the other parameters held fixed. The figures on the right-hand side display the "dispersion" function $\mathscr{D}(\tilde{\nu})$ for the same values of x.

second-degree characteristic equation for λ whose roots have real and imaginary parts that coincide with $\tilde{\kappa}[\mathcal{G}_+(0,x,\Delta,\tilde{\gamma},C,\theta)-1]$ and $\tilde{\kappa}\mathcal{D}_\pm(0,x,\Delta,\tilde{\gamma},C,\theta)$, respectively. The second remark concerns the connection between our present linear stability analysis and the "sidemode gain approach" developed in Ref. 13 and further elaborated on in Ref. 14. This approach is based on the premise that, initially, only a single field mode oscillates strongly; in this situation, one inquires about the possibility that a sideband of very small amplitude can also satisfy the laser oscillation conditions, i.e., that (1) the round-trip phase delay of the sideband be a multiple of 2π and (2) that the gain per round trip be larger than the losses. If a sideband satisfies these conditions, the stationary state is said to be unstable.

A transparent connection between our treatment and the sidemode strategy can be established in the resonant case $\Delta=\theta=0$. In fact, in this case, the sidemode frequencies are determined by equations that coincide with Eq. (30b) with selection of either a plus or minus sign. The function $\mathcal{D}$ can then be interpreted as an anomalous dispersion function. In addition, the sidemode gain turns out to coincide with either $\mathcal{G}_+$ or $\mathcal{G}_-$ [subject to the same sign selection as in Eq. (30b)]. For this reason, in the following we refer to $\mathcal{G}$ as the "gain function." This nomenclature is useful in connection with the identification of the instability domain. In fact, as already emphasized, our procedure allows the identification of the stability boundary, but cannot decide which side of the boundary is the unstable domain. In accord with the sidemode gain approach, we adopt the reasonable point of view that the unstable side of the boundary is the one for which the gain function exceeds unity. This selection agrees with the implications of our first remark and, furthermore, it has never been contradicted in the course of the present work.

Hence, it is undeniable that a useful connection exists between the sidemode approach and our linear stability method. The sidemode strategy lends itself to attractive physical interpretations when dealing with the hole-burning model or with the population pulsation dynamics.[13,14] In our opinion, however, these interpretations should be advanced with some caution for the following reasons. First of all, the sidemode frequencies calculated from Eq. (30b) *do not* coincide with the imaginary parts of the eigenvalues of the linear stability analysis away from the stability boundary. Second, we found examples of solutions $\bar{v}(x)$ of Eq. (30b) such that the corresponding value of the gain is larger than but never equal to unity over the entire range of values of x for which such solutions exist. (An example of this occurrence will be discussed in Sec. VI.) These solutions are not connected with the presence of instabilities of the stationary state and may, in fact, have no physical meaning.

V. OPTICAL BISTABILITY

From now on, in dealing with the Gaussian case we shall confine our attention only to the situation $R/w_0\to\infty$. As shown in Sec. III, the results of the plane-wave theory are recovered in the double limit (17) and (18), so that all cases of practical interest can be regarded as intermediate situations between the limits $R/w_0\to\infty$ and $R/w_0\to 0$.

Depending on the values of C, Δ, and θ, the steady-state curve (7) may or may not be s shaped. There is a very simple link between the character of the stationary curve and the appearance of a zero frequency instability: the instability boundary points at which Eqs. (30) are satisfied for $\tilde{v}=0$ coincide with the turning points of the steady-state curve (if they exist). In fact, as stated in the previous section, $\tilde{\kappa}\mathcal{G}_\pm(0,x,\Delta,\tilde{\gamma},C,\theta)-1$ and $\tilde{\kappa}\mathcal{D}_\pm(0,x,\Delta,\tilde{\gamma},C,\theta)$ coincide with the real and imaginary parts of the two roots of the characteristic equation that emerge in the limit of adiabatic elimination of the atomic variables. This equation has the form[15]

$$\lambda^2+2\kappa\left[1+\frac{2C(1+\Delta^2)}{(1+\Delta^2+x^2)^2}\right]\lambda+\kappa^2\frac{d(y^2)}{d(x^2)}=0\ , \qquad (32)$$

where the function $y^2(x^2)$ is defined by Eq. (7). Hence, if, for example, $\mathcal{G}_+(0,x,\Delta,\tilde{\gamma},C,\theta)-1=\mathcal{D}_+(0,x,\Delta,C,\theta)=0$, we can conclude the Eq. (32) has a root $\lambda=0$. This can only be so when $d(y^2)/d(x^2)=0$, i.e., at the turning points of the steady-state curve. In the case of OB, the instability range for which $\mathcal{G}>1$ coincides with the negative slope segment of the stationary curve (if any exists).

The instabilities of interest in this work are those which arise with nonzero frequency, because they lead to Hopf bifurcations and, possibly, to the occurrence of undamped oscillations. In fact, if the value of the incident field y is such that there is *only one* stationary solution, and this happens to be unstable, the system will approach, of necessity, a regime of steady pulsations which may be regular (periodic or quasiperiodic) or chaotic (completely aperiodic). On the other hand, if the value of the incident field is such that a second stable stationary solution exists, two possible outcomes can be envisioned for the long-term behavior of the system: either stable self-pulsing or approach to the stable stationary state.

Consider the plane-wave case first. As shown in Ref. 16, appropriate choices of the parameters $C,\Delta,\theta,\tilde{\kappa},\tilde{\gamma}$ lead to the identification of an unstable segment of the steady-state curve with positive slope. A necessary condition is that Δ,θ, or both be different from zero. With the possible exception of a small segment of the high transmission branch where the instability causes long-term precipitation into the lower transmission state, the instability of the upper branch leads to undamped self-pulsing behavior. When C is very large, this instability range includes a domain of chaotic behavior which is approached on either side through a sequence of period doubling bifurcations.[17]

The analysis performed in Refs. 16(a) and 16(b) corresponds to the regime of adiabatic elimination of the atomic polarization ($\kappa/\gamma_\perp\to 0$, $\gamma_\parallel/\gamma_\perp\to 0$). On the other hand, a positive-slope instability exists also for nonzero values of $\kappa/\gamma_\perp$ and $\gamma_\parallel/\gamma_\perp$ and for values of C that are within experimental reach.[16(c)] Figure 3(a) shows the domain of the positive-slope instability for $C=75$, $\tilde{\kappa}=0.5$, $\tilde{\gamma}=2$, and several values of Δ and θ. The chosen values of these parameters are compatible with the experiments described in Ref. 18. (Note that the steady-state curve and the stabili-

ty of the stationary states are unaffected by a simultaneous sign change of both Δ and θ.) We have also analyzed the first quadrant of the Δ-θ plane in the range $0 \leq \Delta \leq 10$, $0 \leq \theta \leq 10$, but found no evidence of a positive-slope instability. In Fig. 3(a) we identify a domain in the second quadrant of the Δ-θ plane where the steady-state curve $y = y(x)$ displays a range of positive-slope instability. This domain also includes points for which Δ is equal to zero, corresponding to purely absorptive bistability. On the contrary, no evidence of positive-slope instability was found in the domain $5 \leq \Delta \leq 10$, $-10 \leq \theta \leq 10$ except very near to the axis ($\Delta = 0$).

Consider now the Gaussian case in the limit $R/w_0 \to \infty$. Figure 3(b) shows the domain of positive-slope instability for the same values of the parameters considered in Fig. 3(a). We found no positive-slope instability in the first quadrant of the Δ-θ plane and in the domain $5 \leq \Delta \leq 10$, $-10 \leq \theta \leq 10$. When C is smaller than 100, instabilities are more readily found when Δ and θ have opposite signs, a situation which is less favorable for the observation of bistability.

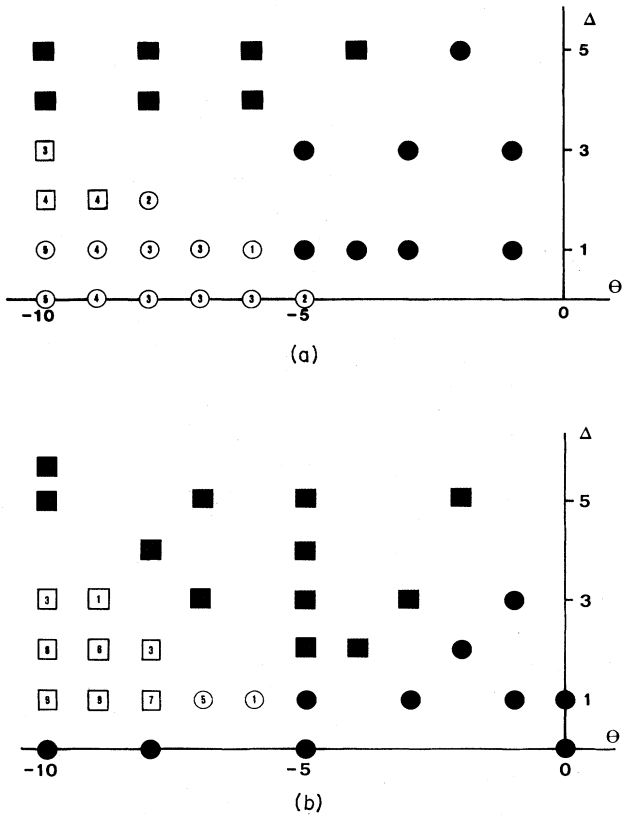

FIG. 3. (a) Optical bistability. Positive-slope instability domain in the Δ-θ plane for the plane-wave case. The parameters used in this scan are $C = 75$, $\tilde{\kappa} = 0.5$, $\tilde{\gamma} = 2$. The black circles indicate that the steady-state curve is s-shaped and that not-positive-slope instability exists for the corresponding values of the parameters. The black squares indicate the absence of bistability *and* instability. The open circles indicate that the steady-state curve is s-shaped and that a range of instability exists whose approximate width Δx is indicated within the circle. Open squares indicate the absence of bistability and the presence of unstable behavior over the approximate range Δx indicated within the square. (b) Same as (a) in the Gaussian case with $R/w_0 \to \infty$.

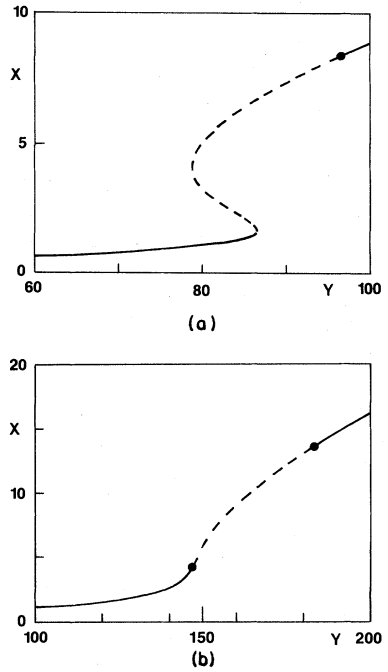

FIG. 4. (a) Optical bistability. Plane-wave case for $C = 75$, $\Delta = 1$, $\theta = -9$, $\tilde{\kappa} = 0.5$, $\tilde{\gamma} = 2$. The graph displays the steady-state transmitted field x as a function of the incident field y. The dashed segment of the curve indicates the unstable domain. (b) Same as (a) in the Gaussian case with $R/w_0 \to \infty$.

In general, the domain of instability in the Δ-θ plane is very nearly the same as in the plane-wave case except that, for $\Delta = 0$, no positive-slope instability appears to exist in the Gaussian case. Figure 3(b) shows that when the steady-state curve $y = y(x)$ acquires an s shape, instabilities are less likely to be found. If we compare the data in Figs. 3(a) and 3(b) for the same values of Δ and θ, we see that the instability range of the x variable is actually larger in the Gaussian case than in the plane-wave limit, as long as Δ is not too small. An example is shown in Fig. 4. The reason for this difference can be traced back to the following fact: in the plane-wave case, the instability range which lies between the two boundary values such that $\mathcal{G}(\bar{v}(x), x, \ldots) = 1$ with $\bar{v}(x) \neq 0$ partly overlaps the negative-slope portion of the stationary curve. On the contrary, the entire steady-state curve has a positive slope for the Gaussian case illustrated in Fig. 4(b). This situation is ideal for observing instabilities because the absence of competitive stable states ensures the emergence of undamped self-pulsing.

VI. LASER WITH INJECTED SIGNAL

This system is the active counterpart of OB. In the following, we shall assume that the parameters have been chosen in such a way that in the absence of an external signal ($y = 0$), the laser is above threshold. In addition, the free-running laser frequency, which is determined by the mode-pulling formula (11), is assumed to be different

from the carrier frequency of the injected field. Under these conditions, the LIS can display undamped oscillations, as shown for the first time in Ref. 19, or chaotic behavior if the incident intensity or the pump parameter are suitably modulated in time.[20] Actually, the laser with injected signal can display chaotic behavior, even when the external parameters are held constant.[21]

For the purpose of this discussion, the atomic and cavity frequencies ω_A and ω_C, respectively, are selected equal to one another, so that the free-running laser frequency also coincides with them. This implies the validity of the relation

$$\Delta/\theta=\tilde{\kappa}\ . \tag{33}$$

A variety of self-pulsing behaviors and routes to chaos, including quasiperiodic, intermittency, and period doubling, have been described in Ref. 21. This same model has also been analyzed[22] in the limit $\kappa/\gamma_\perp\to 0$, $\gamma_\parallel/\gamma_\perp\to 0$ of adiabatic elimination of the atomic polarization, but without restricting the laser to the resonance condition (33). Using parameters that are appropriate for a CO_2 laser, periodic, quasiperiodic, and chaotic pulsations have been obtained. The analyses performed in Refs. 19–22 have all involved the plane-wave approximation. The typical situation with regard to the stationary solutions and the instabilities is illustrated in Figs. 5(a) and 6(a). The steady-state curve, given by Eqs. (7) and (15), has an s shape; no bistability can be observed, however, because the entire segment from the origin to point A is unstable. The value y_A of the incident field plays the role of the injection locking threshold: for $y>y_A$ the driven laser oscillates with the frequency of the injected field. On the other hand, for $y=0$, the laser oscillates at its normal free-running frequency. In the range $0\le y\le y_A$ the long-term output of the system displays undamped pulsations that originate from the competition between the laser and the injected signal.

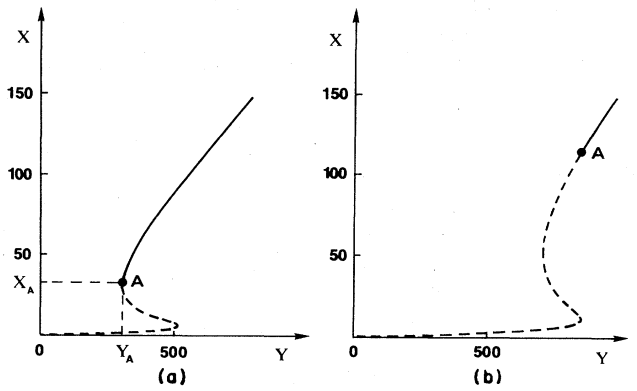

FIG. 5. (a) Laser with injected signal. Plane-wave case for $C=-500$, $\Delta=\theta=5$, $\tilde{\kappa}=\tilde{\gamma}=1$ (note that the resonance condition $\Delta/\theta=\tilde{\kappa}$ is satisfied). Point A marks the boundary of the instability domain (dashed line) and coincides with the injection locking threshold. (b) Same as (a) in the Gaussian case with $R/w_0\to\infty$.

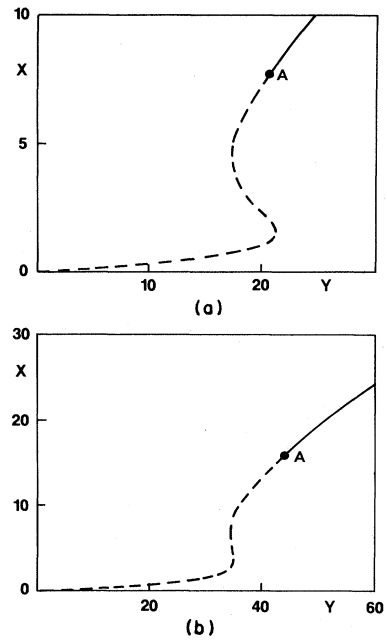

FIG. 6. (a) Laser with injected signal. Plane-wave case for $C=-20$, $\Delta=1$, $\theta=2$, $\tilde{\kappa}=0.5$, $\tilde{\gamma}=0.05$ (note that the resonance condition is satisfied). (b) Same as (a) in the Gaussian case with $R/w_0\to\infty$.

One can distinguish between two situations. In the first, the injection locking threshold A coincides with the left turning point of the steady-state curve [Fig. 5(a)]; in the second, point A lies in the upper part of the s-shaped curve [Fig. 6(a)]. In the latter case, as y approaches y_A from below, the amplitude of the undamped oscillations decreases continuously, and A is a Hopf bifurcation point. Under this condition, Eq. (30b) has two symmetric nonzero solutions for $y=y_A$ such that the gain function equals unity. On the other hand, when A coincides with the left turning point, and y approaches y_A from below, the system exhibits a spiking behavior with a temporal separation between the spikes that apparently diverges as $y\to y_A$.[21] Under this condition, Eqs. (30) have no solutions for $\tilde{\nu}\neq 0$. Actually, a wide range of values of x exists for which Eq. (30b) has nonzero solutions; the corresponding value of the gain, however, is always larger than but never equal to unity. This is an example of the situation mentioned at the end of Sec. IV.

Regardless of the position of point A, the turning points of the steady-state curve are instability boundaries at which Eqs. (30) are satisfied, as usual, for $\tilde{\nu}=0$. To be more precise, in the case of LIS *two* instability ranges of this kind exist, according to Eqs. (30), depending on the selection of the plus or minus signs. One of the two ranges coincides with the lower branch of the stationary curve from $y=0$ to the right turning point, the other covers the entire steady-state curve from the origin to the left turning point including the segment with negative slope.

Consider now the LIS in the case of a Gaussian profile with $R/w_0\to\infty$. Figures 5(b) and 6(b) show the steady-state curve obtained from Eqs. (7) and (8) and the instability range for the same values of the parameters used in

Figs. 5(a) and 6(a), respectively. For both Figs. (5) and (6) the instability range turns out to be much wider in the Gaussian case, and point A, which lies in the upper branch, corresponds to a Hopf bifurcation. The significant broadening of the instability domain can be understood qualititatively as follows. As one can see from the Appendix, in the limit $R/w_0 \to \infty$, the functions $\mathscr{A}$ and $x^2\mathscr{B}$ which are the building blocks of Eqs. (30) are obtained by averaging the corresponding plane-wave functions over the profile of the output intensity [see Eqs. (A7)] from zero to the actual value of x. Hence, the behavior of LIS or OB in the presence of a Gaussian profile can be viewed as an average of the plane-wave limit. When dealing with the plane-wave version of LIS, the gain function $\mathscr{G}$ is larger than unity for x ranging from zero to x_A. In the Gaussian case, even when x exceeds the plane-wave value of x_A, there is a considerable range of values of the output field which are smaller than x_A, but still such that the plane-wave gain is larger than unity. Hence, in carrying out the average, the Gaussian gain turns out to be larger than unity, at least as long as x does not become too large. The implication is that the injection locking threshold x_A in the Gaussian case is pushed to higher values. This is just the opposite of what was discussed in Ref. 4(a), where the instability domain was seen to disappear in the Gaussian case because of the dominance of the stable contributions on the averaged result when $R/w_0 \to \infty$.

VII. ORDINARY LASER

This is, to our knowledge, the first quantum optical system for which a self-pulsing instability was predicted. As shown by Haken and co-workers,[23,24] this instability arises under "bad cavity" conditions (i.e., $\kappa > \gamma_{\parallel} + \gamma_{\perp}$) and requires laser operation well above the ordinary threshold. In the resonant case $\Delta = -\theta = 0$, and for $y = 0$, the laser model (5) becomes equivalent[25] to the well-known Lorentz model[26] of hydrodynamics. Therefore, the instability threshold corresponds to a subcritical Hopf bifurcation which eventually leads to the appearance of chaotic behavior. More recently, the detuned laser ($\Delta = -\theta \neq 0$) has also been studied.[10] By analytical means, Ref. 10 contains proof that when the detuning Δ becomes sufficiently large, the instability threshold becomes a supercritical Hopf bifurcation, which leads to the smooth appearance of a periodic self-pulsing state.

Consider now the matter of instabilities in the case of the Gaussian beam profile and $R/w_0 \to \infty$. In studying Eqs. (30) we take into account Eq. (9) and the relation (11) that connects C with x for the FRL. For any value of x, Eqs. (30) are satisfied by the solution $\tilde{v} = 0$, i.e., $\lambda = 0$ is always an eigenvalue of the laser stability problem. This is a well-known general fact which is connected to the arbitrariness of the phase in steady state.

As usual, we are interested in seeking nonzero solutions of Eqs. (30) because they correspond to the emergence of Hopf bifurcations. The resonant case $\Delta = -\theta = 0$ was already studied in Ref. 4(b) with the conclusion that no such solution existed because $\mathscr{G}$ is always smaller than unity. By holding $\tilde{\kappa}$ and $\tilde{\gamma}$ fixed at the values $\tilde{\kappa} = 5$, $\tilde{\gamma} = 1$ we have analyzed the cases $\Delta = -\theta = 1,5,10$ and found that the gain function $\mathscr{G}$ indeed becomes larger than unity over sizeable ranges of the $\tilde{v}$ variable without, however, the appearance of nonzero solutions. The implication is that for these values of the parameters, the nontrivial stationary solution is stable over its entire domain of existence.

Of course, this does not exclude that one can find an instability in the Gaussian case for different values of the parameters. Furthermore, our calculations have been carried out in the limit $R/w_0 \to \infty$. If one should decrease this ratio gradually, while holding C' fixed [see Eq. (18)], one recovers the plane-wave theory and therefore also the unstable behavior.

Regular and chaotic self-pulsing behavior has been observed extensively in inhomogeneously broadened lasers[27,28] even in the vicinity of the lasing threshold. The instability problem in such lasers including a Gaussian transverse profile will be considered in future work.

VIII. CONCLUSIONS

We have undertaken an extensive analysis of the steady-state behavior and instabilities for three distinct optical systems, namely, optical bistability, the laser with injected signal, and the free-running laser. These systems have all been described in a unified way by the same homogeneously broadened atomic model. The goal of our analysis was to clarify the role played by a transverse Gaussian intensity profile inside the optical cavity and to compare the results with those of earlier studies in which the electromagnetic field was assumed to have a uniform plane-wave cross-sectional shape. In our study of the instabilities we focused our attention on atomic samples having transverse dimensions that are much larger than the beam waist, because this configuration is essentially opposite to that of a plane-wave geometry.

In the cases of optical bistability and the laser with injected signal we found that the domain of instability in control parameter space is notably widened relative to the plane-wave limit. This is just the opposite of what was previously found in the case of other laser instabilities.[4]

In view of the possible realization of an all-optical clock, the results of our analysis of the OB problem appear rather promising. For $C = 75$, the instability range seems large enough to be experimentally accessible. In this range the optimum configuration calls for values of the atomic and cavity mistuning which have opposite signs. Further improvements are predicted in the absence of bistability when the steady-state curve is single valued and the existence of an instability implies also the existence of undamped pulsations.

In the case of the laser with injected signal the Gaussian profile leads to a remarkable increase of the threshold level for injection locking. This effect arises in part from the fact that the left turning point of the steady-state curve is shifted towards a higher value of the driving field and in part from the broadening of the instability range itself in the upper branch. If the numerical simulation of the equations of motion in the Gaussian case should confirm the possibility of chaotic behavior for moderate values of $|C|$, there is little doubt that LIS would have to be regarded as an ideal candidate for an experimental

study of the chaotic regime and of the routes to chaos in quantum optical systems. In the case of the free-running laser we were not able to demonstrate the existence of parameters that would lead to an instability for the nontrivial steady-state solution, in line with the results obtained in Ref. 4(b) for the resonant case.

In general, we believe that the instability problem including transverse effects is not just an extension, or generalization, of the plane-wave theory, but rather an independent study of its own. In fact, there are examples of plane-wave instabilities that disappear in the Gaussian case[4] and instabilities that are absent in the plane-wave limit and which arise in the context of a full two-dimensional model.[5] The present lively interest in instability effects in quantum optical systems and especially in their experimental realization requires on the one hand further developments of the present theoretical investigations, and on the other, the identification of suitable experimental tools (one might like to call them "transverse spectroscopy") in order to pin down the role of the radial profile on these and related phenomena. It is likely that only simultaneous advances along these lines will lead to a satisfactory understanding of most unstable behaviors in quantum optical systems.

ACKNOWLEDGMENTS

This work has been carried out in the framework of an operation launched by the Commission of the European Communities under the experimental phase of the European Community Stimulation Action (1983–1985). The work has also been partially supported by the Italian National Research Council (Consiglio Nazionale delle Ricerche) by the U.S. Army Research Office, and by the Research Laboratories of the Martin-Marietta Corporation. Travel support during this work has been partially supported by North Atlantic Treaty Organization (NATO) under Grant No. 866-83. One of us (R.J.H.) is grateful for a grant provided by the International Centre for Theoretical Physics (Trieste) Program for Training and Research in Italian Laboratories.

APPENDIX

The linearized equations (20) can be solved, for example, by the Laplace-transform method. Owing to the presence of the radial integrals, the Laplace transforms of the fluctuations $\delta f(t)$ and $\delta f^*(t)$ may develop cuts in the complex plane in addition to the expected poles. In seeking solutions of the type given by Eq. (21) we are considering only the contributions due to the poles of the Laplace-transform variables. This is equivalent to assuming that the contributions from the cuts decay in time and, therefore, do not give rise to instabilities.

We now produce explicit expressions for the functions $\mathscr{A}$ and $\mathscr{B}$ that appear in Eqs. (23). It is convenient to start from the plane-wave limit in which the function $\mathscr{A}$ takes the form

$$\mathscr{A}^{(\mathrm{pw})}(\tilde{\nu},x,\Delta,\tilde{\gamma})=\frac{m_1x^4+n_1x^2+q_1}{(1+\Delta^2+x^2)(ax^4+bx^2+c)} . \tag{A1}$$

The various symbols on the right-hand side of Eq. (A1) are defined as follows:

$$m_1=-\frac{\tilde{\gamma}^2}{2}i\tilde{\nu}(1+i\Delta)(1-i\tilde{\nu}) , \tag{A2a}$$

$$n_1=\tilde{\gamma}\left\{i\frac{\tilde{\nu}}{2}(1+i\Delta)(\sigma_1-i\sigma_2)\right.$$
$$+(1+\Delta^2)\{\tilde{\gamma}-\tilde{\nu}(\tilde{\nu}-\Delta)$$
$$\left.+i[\tilde{\nu}+\tilde{\gamma}(\tilde{\nu}-\Delta)]\}(1-i\tilde{\nu})\right\} , \tag{A2b}$$

$$q_1=(1+\Delta^2)(\sigma_1-i\sigma_2)\{\tilde{\gamma}-\tilde{\nu}^2+\tilde{\nu}\Delta+i[\tilde{\nu}+\tilde{\gamma}(\tilde{\gamma}-\Delta)]\} ; \tag{A2c}$$

$$a=\tilde{\gamma}^2(1+\tilde{\nu}^2) , \tag{A3a}$$

$$b=2\tilde{\gamma}(\sigma_1+\sigma_2\tilde{\nu}) , \tag{A3b}$$

$$c=\sigma_1^2+\sigma_2^2 ; \tag{A3c}$$

where

$$\sigma_1=-\tilde{\nu}^2(\tilde{\gamma}+2)+\tilde{\gamma}(1+\Delta^2) , \tag{A4a}$$

$$\sigma_2=\tilde{\nu}(-\tilde{\nu}^2+1+\Delta^2+2\tilde{\gamma}) . \tag{A4b}$$

The function $\mathscr{B}$ instead takes the form

$$x^2\mathscr{B}^{(\mathrm{pw})}(\tilde{\nu},x,\Delta,\tilde{\gamma})\frac{m_2^2x^4+n_2x^2+q_2}{(1+\Delta^2+x^2)(ax^4+bx^2+c)} , \tag{A5}$$

where

$$m_2=-\frac{\tilde{\gamma}^2}{2}[2+\tilde{\nu}\Delta+i(\tilde{\nu}-2\Delta)](1-i\tilde{\nu}) , \tag{A6a}$$

$$n_2=-\frac{\tilde{\gamma}}{2}(\sigma_1-i\sigma_2)[2+\tilde{\nu}\Delta+i(\tilde{\nu}-2\Delta)] , \tag{A6b}$$

$$q_2=0 . \tag{A6c}$$

Note that a,b,c are real, while m_i, n_i, and q_i $(i=1,2)$ are complex.

In the case of the Gaussian intensity profile, by taking into account the radial integrals we obtain

$$\mathscr{A}(\tilde{\nu},x,\Delta,\tilde{\gamma})=\frac{1}{x^2}\int_{x^2e^{-2(R/w_0)^2}}^{x^2}d\rho\,\mathscr{A}^{(\mathrm{pw})}(\tilde{\nu},\rho^{1/2},\Delta,\tilde{\gamma}) , \tag{A7a}$$

$$x^2\mathscr{B}(\tilde{\nu},x,\Delta,\tilde{\gamma})=\frac{1}{x^2}\int_{x^2e^{-2(R/w_0)^2}}^{x^2}d\rho\,\rho\mathscr{B}^{(\mathrm{pw})}(\tilde{\nu},\rho^{1/2},\Delta,\tilde{\gamma}) , \tag{A7b}$$

where the functions $\mathscr{A}^{(\mathrm{pw})}(\tilde{\nu},\rho^{1/2},\Delta,\tilde{\gamma})$ and $\mathscr{B}^{(\mathrm{pw})}(\tilde{\nu},\rho^{1/2},\Delta,\tilde{\gamma})$ that appear on the right-hand side of Eqs. (A7) are obtained from Eqs. (A1) and (A5), respectively, by setting $x^2=\rho$.

Thus, from Eqs. (A7a) and (A1) we obtain the following explicit expression for $\mathscr{A}$:

$$\mathscr{A}(\tilde{\nu},x,\Delta,\tilde{\gamma})=\frac{1}{x^2}\left\{A_1\ln\left[\frac{1+\Delta^2+x^2}{1+\Delta^2+x^2\exp[-2(R/w_0)^2]}\right]\right.$$
$$+\frac{B_1}{2a}\ln\left[\frac{ax^4+bx^2+c}{ax^4\exp[-4(R/w_0)^2]+bx^2\exp[-2(R/w_0)^2]+c}\right]$$
$$+\left[C_1-\frac{bB_1}{2a}\right]\frac{2}{(4ac-b^2)^{1/2}}\left[\arctan\left[\frac{2ax^2+b}{(4ac-b^2)^{1/2}}\right]\right.$$
$$\left.\left.-\arctan\frac{2ax^2\exp[-2(R/w)^2]+b}{(4ac-b^2)^{1/2}}\right]\right\}, \tag{A8}$$

where

$$(4ac-b^2)^{1/2}=2\tilde{\gamma}\,|\,\sigma_1\tilde{\nu}-\sigma_2\,| \tag{A9}$$

and A_1, B_1, and C_1 are solutions of the linear system

$$\begin{aligned} &aA_1+B_1=m_1\ , \\ &bA_1+(1+\Delta^2)B_1+C_1=n_1\ , \\ &cA_1+(1+\Delta^2)C_1=q_1\ . \end{aligned} \tag{A10}$$

The explicit expression of $x^2\mathscr{B}(\tilde{\nu},x,\Delta,\tilde{\gamma})$ is given again by Eq. (A8) with A_1, B_1, and C_1 replaced by A_2, B_2, and C_2. These are solutions of a linear system which is formally identical to the one in Eqs. (A10) except for the replacement of m_1, n_1, and q_1 by m_2, n_2, and q_2.

*Permanent address: Departamento de Fisica Pontifícia Universidade Católica do Rio de Janeiro, 20000 Rio de Janeiro, Brazil.

[1]R. J. Ballagh, J. Cooper, M. W. Hamilton, W. J. Sandle, and D. M. Warrington, Opt. Commun. **37**, 143 (1981).

[2]J. V. Moloney, F. A. Hopf, and H. M. Gibbs, Phys. Rev. A **25**, 3442 (1982); J. V. Moloney, H. M. Gibbs, and F. A. Hopf, in *Proceedings of the Topical Meeting on Optical Bistability, Rochester, N.Y., 1983,* edited by C. M. Bowden, H. M. Gibbs, and S. L. McCall (Plenum, New York, 1984).

[3]W. J. Firth and E. M. Wright, Phys. Lett. **92**, 211 (1982).

[4]L. A. Lugiato and M. Milani, Z. Phys. B **50**, 171 (1983); Opt. Commun. **46**, 57 (1983); in *Proceedings of the Topical Meeting on Optical Bistability, Rochester, N.Y., 1983* edited by C. M. Bowden, H. M. Gibbs, and S. L. McCall (Plenum, New York, 1984).

[5]R. Hauck, F. Hollinger, and H. Weber, Opt. Commun. **47**, 141 (1983).

[6]K. Ikeda, Opt. Commun. **30**, 257 (1979); K. Ikeda, H. Daido, and D. Akimoto, Phys. Rev. Lett. **45**, 709 (1980).

[7]R. Bonifacio and L. A. Lugiato, Lett. Nuovo Cimento **21**, 505 (1978).

[8]E. Arimondo, A. Gozzini, F. Lovitch, and E. Pistelli, in *Optical Bistability,* edited by C. M. Bowden, M. Ciftan, and H. R. Robl (Plenum, New York, 1981).

[9]P. D. Drummond, IEEE J. Quantum Electron. **QE-17**, 301 (1981).

[10]P. Mandel and H. Zeghlache, Opt. Commun. **47**, 146 (1983).

[11]R. Bonifacio and L. A. Lugiato, Lett. Nuovo Cimento **21**, 517 (1978).

[12]M. Marsden, *The Geometry of the Zeros of a Polynomial in a Complex Variable,* Math Surveys No. 3 (American Mathematical Society, New York, 1949).

[13]L. W. Casperson, Phys. Rev. A **21**, 911 (1980); **23**, 248 (1981).

[14]S. T. Hendow and M. Sargent III, Opt. Commun. **40**, 385 (1982); **43**, 59 (1982).

[15]L. A. Lugiato, *Theory of Optical Bistability,* in Vol. 21 of *Progress in Optics,* edited by E. Wolf (North-Holland, Amsterdam, 1984), p. 104.

[16](a) L. A. Lugiato, L. M. Narducci, D. K. Bandy, and C. A. Pennise, Opt. Commun. **43**, 281 (1982); (b) L. M. Narducci, D. K. Bandy, C. A. Pennise, and L. A. Lugiato, *ibid.* **44**, 207 (1983); (c) L. A. Lugiato and L. M. Narducci, in *Coherence and Quantum Optics V,* edited by L. Mandel and E. Wolf (Plenum, New York, 1984); see also K. Ikeda and O. Akomoto, Phys. Rev. Lett. **48**, 617 (1982).

[17]R. M. May, Nature (London) **261**, 459 (1976); S. Grossmann and S. Thomae, Z. Naturforsch. **32a**, 1353 (1977); M. J. Feigenbaum, J. Stat. Phys. **19**, 25 (1978).

[18]D. E. Grant and H. J. Kimble, Opt. Lett. **7**, 353 (1982); see also Opt. Commun. **44**, 415 (1983).

[19]M. B. Spencer and W. E. Lamb, Jr., Phys. Rev. A **5**, 884 (1972).

[20]T. Yamada and R. Graham, Phys. Rev. Lett. **45**, 1322 (1980); M. J. Scholz, T. Yamada, H. Brand, and R. Graham, Phys. Lett. **82A**, 321 (1981).

[21]L. A. Lugiato, L. M. Narducci, D. K. Bandy, and C. A. Pennise, Opt. Commun. **46**, 64 (1983); D. K. Bandy, L. M. Narducci, C. A. Pennise, and L. A. Lugiato, in *Coherence and Quantum Optics V,* edited by L. Mandel and E. Wolf (Plenum, New York, 1984).

[22]F. T. Arecchi, G. L. Lippi, G. Puccioni, and J. Tredicce, in *Coherence and Quantum Optics V,* edited by L. Mandel and E. Wolf (Plenum, New York, 1984).

[23]H. Haken, Z. Phys. **190**, 327 (1966).

[24]H. Risken, C. Schmidt, and W. Weidlich, Z. Phys. **194**, 337 (1966).

[25]H. Haken, Phys. Lett. **53A**, 77 (1975).

[26]E. N. Lorenz, J. Atmos. Sci. **20**, 130 (1963).

[27]L. W. Casperson, IEEE J. Quantum Electron. **QE-14**, 756 (1978).

[28]R. S. Gioggia and N. B. Abraham, Phys. Rev. Lett. **51**, 650 (1983) and references therein.